All Theses and Dissertations

2015-03-01

Experimental and Numerical Study of High-Speed Friction Stir Spot Welding of Advanced High-Strength Steel

Utsab Karki
Brigham Young University - Provo

Follow this and additional works at: https://scholarsarchive.byu.edu/etd

Part of the Industrial Engineering Commons

Experimental and Numerical Study of High-Speed Friction Stir Spot Welding of

Advanced High-Strength Steel

Utsab Bikram Karki

A thesis submitted to the faculty of
Brigham Young University
in partial fulfillment of the requirements for the degree of

Master of Science

Mike P. Miles, Chair
Charles R. Harrell
Andy R. George

School of Technology

Brigham Young University

February 2015

ABSTRACT

Experimental and Numerical Study of High-Speed Friction Stir Spot Welding of
Advanced High-Strength Steel

Utsab Bikram Karki
School of Technology, BYU
Master of Science

With the desire to lighten the frame while keeping or increasing the strength, Advanced
High-Strength Steels (AHSS) have been developed for use in the automotive industry. AHSS
meet many vehicle functional requirements because of their excellent strength and acceptable
ductility. But joining AHSS is a challenge, because weldability is lower than that of mild steels.
Friction stir spot welding (FSSW) is a solid state joining process that can provide a solution to
the weldability issues in AHSS, but FSSW has not been studied in great detail for this
application.

In this work, Si_3N_4 tools were used for FSSW experiments on DP 980 steel with 1.2mm
thickness. Joint strength was measured by lap shear tension testing, while thermocouples were
used for the temperature measurements. A finite element model was developed in order to
predict material flow and temperatures associated with FSSW. Since a 3D model of the process
is very time consuming, a novel 2D model was developed for this study. An updated Lagrangian
scheme was employed to predict the flow of sheet material, subjected to the boundary conditions
of the fixed backing plate and descending rotating tool. Heat generation by friction was
computed by including the rotational velocity component from the tool in the thermal boundary
conditions. Material flow was calculated from a velocity field while an isotropic, viscoplastic
Norton-Hoff law was used to compute the material flow stress as a function of temperature,
strain and strain rate. Shear stress at the tool/sheet interface was computed using the viscoplastic
friction law.

The model predicted welding temperatures to within 4% of the experiments. The welding
loads were significantly over predicted. Comparison with a 3D model of FSSW showed that
frictional heating and the proportion of total heat generated by friction were similar. The position
of the joint interface was reasonably well predicted compared to experiment.

Keywords: Utsab Karki, high speed friction stir spot welding, simulation, DP 980, Si_3N_4 tool,
advanced high strength steel

ACKNOWLEDGEMENTS

TABLE OF CONTENTS

LIST OF TABLES

+

LIST OF FIGURES

1 INTRODUCTION

1.1 Background

Friction stir spot welding (FSSW) joins two metal sheets by plunging a rotating tool consisting of a pin and a shoulder. The pin and shoulder can be of different designs. The pin can be a standard cylindrical, triangular, tapered, or an inverse tapered. The shoulder can be smooth or threaded, and have a flat, concave, tapered or a convex shape.

FSSW has been successfully applied on aluminum and its alloys, which have led to significant energy and cost savings especially on automotive industries. This process is energy efficient and uses non-consumable tool. FSSW has proven to reduce the manufacturing cost in aluminum alloys compared to other welding processes such as Resistance Spot Welding (RSW), and laser spot welding. Although, the process is perceived to be a simple process, the physics involved is complex and many studies are yet to be performed to gain full understanding of the process.

Mazda Motor Corporation used the FSSW process on the rear door of Mazda RX-8 in 2003. They reported more than 90% energy savings and over 40% investment reduction, when compared to the traditional RSW (Feng, 2005). AHSS has gained a lot of attention in the automotive industry. Not a lot of research has been conducted on AHSS rotating at speeds over

2000 rpm. Gaining more understanding in this area will help the automotive industry in making lighter and stronger automobiles.

1.1.1 RSW of AHSS

The properties of friction stir spot welds have gained attention from the automotive industry for joining AHSS because the bonding process is solid state. This process avoids some of the issues related to the melting and solidification of the weld pool. The current, primary welding process of auto body structure, RSW, may not be able to achieve the full benefits of AHSS. This is because of the high cooling rate and the shrinkage cracks that occur, resulting in a brittle microstructure with questionable durability (Oikawa, 2006).

1.1.2 High Speed FSSW of AHSS

There has been a huge success in the FSSW of aluminum and its alloys. But there are many difficulties in applying the same technology to AHSS. Solid state bonding and the appearance of the weld, lap-weld without bulk melting, has gained a huge attention from automotive industries.

The current oil crisis and higher safety standards set by the National Highway Traffic Safety Administration (NHTSA) have put pressure on automobile manufacturers to find a better way to make automobiles lighter and stronger. Automakers have incorporated AHSS into the structural and safety components of the vehicle. Honda was the first one to put high grade AHSS into a vehicle body, thus supporting their initiative towards safety and environmental leadership (Feng, 2005).

At present, there is limited data available on the mechanical and micro structural properties of high speed FSSW of AHSS. The tools used for experimentation are mostly made from silicon nitride, polycrystalline cubic boron nitride (PCBN), and PCBN/ Tungsten/ Rhenium composites. A large number of experiments need to be conducted with various parameters in order to understand which material lasts longer. Sometimes the tool lasts longer whereas other times the tool made of the same materials cracks after few hundred welds. Individual tooling can costs as much as $2500 and the time involved in testing has generated tremendous interest in finding alternate methods for experiments (Ridges, 2011).

1.1.3   Simulation of High Speed FSSW

Different two-dimensional (2D) and three-dimensional (3D) numerical models for Friction Stir Welding (FSW) capable of predicting successful results have been reported. However, there has been less effort on the development of reliable numerical model on FSSW. There are a few numerical models with aluminum and its alloys but none related to AHSS. Numerous experiments need to be conducted to verify and validate the numerical models so that correct results can be obtained for different parameters in the process.

1.2   Contribution of This Study

The purpose of the research is to model the FSSW process for Dual Phase (DP) 980 steel using a 2D approach within the finite element method framework. The model would be focused in accurately predicting the flow of material during the welding process, as well as the welding temperatures. Predictions will be compared to experiments for validation. The study will use

tools with concave shoulder for performing the welds. The AHSS used for the testing is DP 980 steel.

1.3   Hypotheses

The hypotheses for this research are as follows:

- The joint interface shape can be predicted accurately (position within 5-10%) using a 2D finite element approach

- Peak temperatures and temperature distribution (within 5-10%) at 3, 4, and 6.5 mm from the center of the weld can be predicted using the numerical model

1.4   Significance of the Study

The significance of this study lies in the potential to understand the process parameters (rpm, plunge rate, and plunge depth) that affect the bond strength. The temperature predictions at various locations during the FSSW process have the potential of providing an understanding of the diffusion bonding process that occurs during welding. While this study is focused primarily on the prediction of welding temperatures and material flow in the joint, the end goal will be to use the process simulation to predict bond area. This will be done by using data from diffusion bonding experiments, to be done in future work, to correlate welding temperatures, joint line pressure, and time to the bonding process. Such a prediction will facilitate the development of FSSW as a tool for spot welding of AHSS.

1.5 Delimitations

In this study, only one tool design with concave shoulder was used. The test included four different rpm speeds: 3000, 4000, 5000 and 6000. The welding tool was made of Si_3N_4 material. The coupons used for the spot welding test were DP 980 steel coupons of 100 x 25 x 1.2 mm. The testing was performed on one machine only in order to remove the measureable variability in backlash and accuracy. Since weld strength was found to be highly sensitive to small parameter variations, the process was made as consistent possible. Similar thermocouples were used to measure the temperatures at various locations.

1.6 Definition of Terms

DP 980 Steel: Dual Phase steel consisting of martensitic and ferritic microstructure with an ultimate tensile strength of 980 MPa

Friction Stir Spot Welding (FSSW): A spot welding process that uses a non-consumable tool to weld two sheets mostly by generation of friction and plastic deformation

Nugget: The portion of the friction weld that corresponds to the location of pin and undergoes heavy deformation, resulting significant change in the microstructure. Also called Stir Zone.

Lap Shear Strength: The strength of a welded joint under tensile test

Heat Affected Zone (HAZ): The portion of the friction weld that undergoes changes in the microstructure due to heat and lies in between base material and TMAZ

Plunge Depth: The distance, measured in mm, at which the tool penetrates into the metal coupons

Plunge Rate: The speed, measured in mm/s, at which the tool penetrates into the metal coupons

RPM: Revolutions per minute (rpm). Rotational speed of the tool used during the welding cycle

Thermo Mechanically Affected Zone (TMAZ): The portion of the friction weld that undergoes small deformation and changes in the microstructure due to plastic deformation. Can be found in between nugget and HAZ

Welding Parameters: A set of parameters that includes plunge rate, plunge depth and rotational speeds to produce a weld

2   LITERATURE REVIEW

2.1   Overview

Mazda reported the first mass production application of FSSW and used it on the rear door of the 2003 RX-8. Success with aluminum and its alloys in this process has recently led a huge interest in its application to AHSS. Other joining methods such as RSW do not always deliver acceptable results and maintain the characteristics desired for welding AHSS (Santella, 2010). A few numerical models were tested with the aluminum with an rpm of less than 2000, but none have been tested at high rpms and with AHSS.

2.2   Microstructure of the Welds

Tests were conducted on FSSW joints made of aluminum 6082-T6 alloys. The welding caused change in mechanical properties depending on the distance from the center. In the paper, dimensions of different zones were obtained from the experimental specimens whereas the zones' shapes were assumed from literature. Stir zone had complete recrystallization, material were modified mechanically and thermically in thermo mechanical affected zone (TMAZ). Material was affected by heat dissipated in heat-affected zone (HAZ), which was also an axial symmetric one and material beyond this zone was not modified. Material hardness decreased coming from the base material to the weld center (Fanelli, 2012).

Three common microstructure zones were observed in all DP 800 steel welds: TMAZ, HAZ and the base material. TMAZ zone showed acicular martensite structure. The material in this zone was fully austenized on heating and high cooling rate resulted in full martensite microstructure. HAZ showed a ferrite/martensite structure in very fine scale. Due to high temperature in the stir zone, the region had phase transformation to form fine grain structure; the ferrite transformed to austenite upon heating. On cooling, it transformed back to ferrite in finer scale. The parent material consisted of islands of martensite within continuous ferrite matrix (Al-Shahrani, 2010).

2.3   **Tool Design and Strength of the Welds**

The hook geometry from the numerical model closely matched the experimental results. The hook formation for the tapered pin was smaller than the standard cylindrical pin whereas the standard deviation of particles was similar. For the inverse tapered pin, both the hook formation and the standard deviation of particles were similar to the standard pin (Miles, 2014). For the convex shoulder, there was no hook formation, but the standard deviation of particles was small, indicating the weld strength to be lower than the standard cylindrical pin. Sharp hook was observed for the concave shoulder but the standard deviation was smaller. For the triangular pin with a concave shoulder, there were sharp hook and high standard deviation in comparison to the standard pin. Tool shoulder profile had a great impact on the material mixing and weld strength. The triangular pin with a concave shoulder was considered to yield high strength welds compared to other designs (Hirasawa, 2010).

2.4   **Numerical Model of FSSW**

The FE model had work piece, tool and backing anvil. The tool and the anvil were modeled as analytical rigid surfaces; the mesh was denser at the center of the work piece. The numerical and the experimental result differ by about 5.1%. Based on FE results, the heat generated due to friction at the tool and top work piece contributed 96.84% of the total energy. Similarly, about 0.02% of the total was due to the frictional force at the interface between the top and the bottom work pieces and the remaining 3.14% was due to the internal friction/plastic work. Higher rotational speed results in the higher velocity of the material and as a result higher energy was produced. The frictional dissipation energy was reduced by about 8.4% when the rotational speed was reduced from 3000– 2500 rpm, and reduced by about 19.2% when it is reduced from 3000–2000 rpm. There was an inverse correlation between the plunge rate and the frictional as well as plastic dissipation energy (Awang, 2010).

A simplified isothermal 3D FE model of just the initial plunge phase of the FSSW process was created to compare the results against the experimental results with similar tool geometry, sequence of operations, and process parameters. The experiment consisted of four processes in which the pin and the shoulder moved at different velocities. The dimensions of some of the parts were shortened from the original values in order to reduce the computational time. The two plates were modeled as a single plate. The pin was modeled as a rigid body. Since only the first two stages were considered for this paper, the shoulder was not included in the simulation. The motion of the pin was constrained in all directions except for the translation and rotation about the vertical axis. The bottom face of the plate was constrained in y, the right and left faces in the x, and the front and the back in the z. The plate for the model was 0.25 in. thick whereas in the experiment two 0.080 in. plates were used. The temperature of the material was taken as 800 F in

the model and it was approximately about 850 F in the experiment. All other parameters were the same. The experiment was run at 800 rpm and the flash generated during the plunge test was similar to the one from the model. The vertical plunge forces as the function of the plunge distance predicted by the model were close to the ones obtained from the experiment (Muci-Küchler, 2005).

An average value of characteristics for each zone was applied to the FE model, obtaining some discontinuity properties at border zones. Although the variation was sharp, it was similar to the variation in mechanical characteristics from one zone to the other in FSSW. Matching the results from the experiments to the numerical data validated the model. That allowed evaluating the main parameters that influence the mechanical behavior and strength of the FSSW joints (Fanelli, 2012).

3   METHODOLOGY

3.1   **Introduction**

Concave shouldered Si_3N_4 tools as shown in Figure 3-1 were used for the Friction Stir Spot Welding (FSSW) of DP 980 coupons. The tool had a shoulder diameter and pin length of 10 mm and 3 mm respectively.

Figure 3-1 FSSW Tool

3.2 Weld Parameter Development

To simplify the comparison between experiments and numerical models, welding parameters were developed for a simple plunge, at a constant rate, and without any dwell time. The parameters included rpm, plunge rate and plunge depth.

Table 3-1 Process Parameters Used in the Experiment and Simulation

Tool Rotation (rpm)	Plunge Rate (mm/s)	Plunge Depth (mm)	Sheet Thickness (mm)
3000			
4000	0.106	2.5	1.2
5000	0.212		
6000			

3.3 Experimental Design

Spot welds were produced on DP 980 coupons with 100 mm × 25 mm × 1.2 mm dimensions and with an overlap of 25 mm. The steel consisted of ferrite matrix with islands of martensite. The spot weld was positioned on the center of the overlap.

(a)

(b)
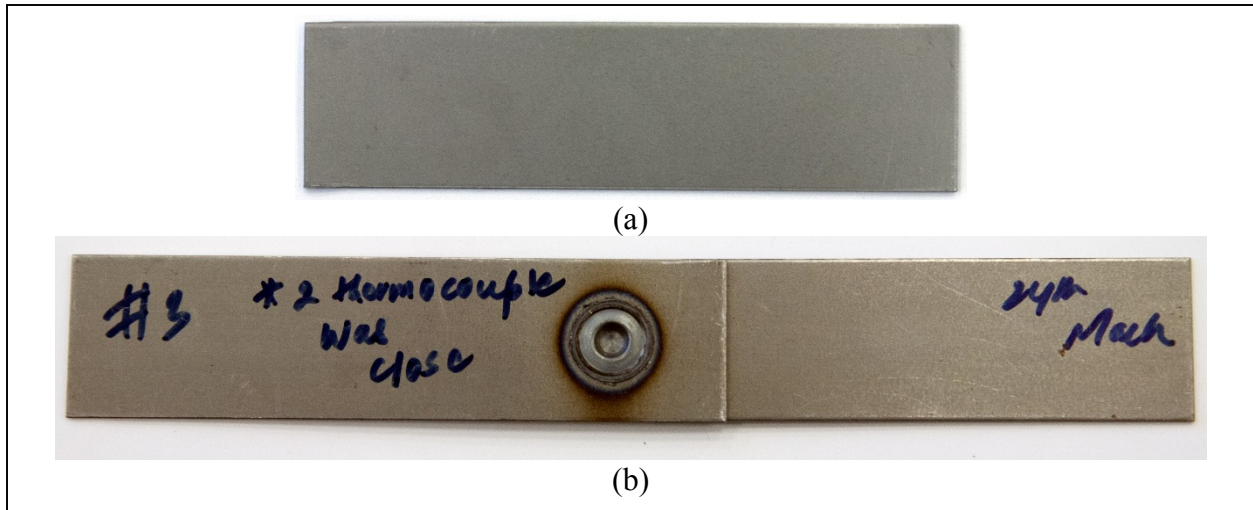
Figure 3-2 (a) Single Coupon (b) Welded Coupons
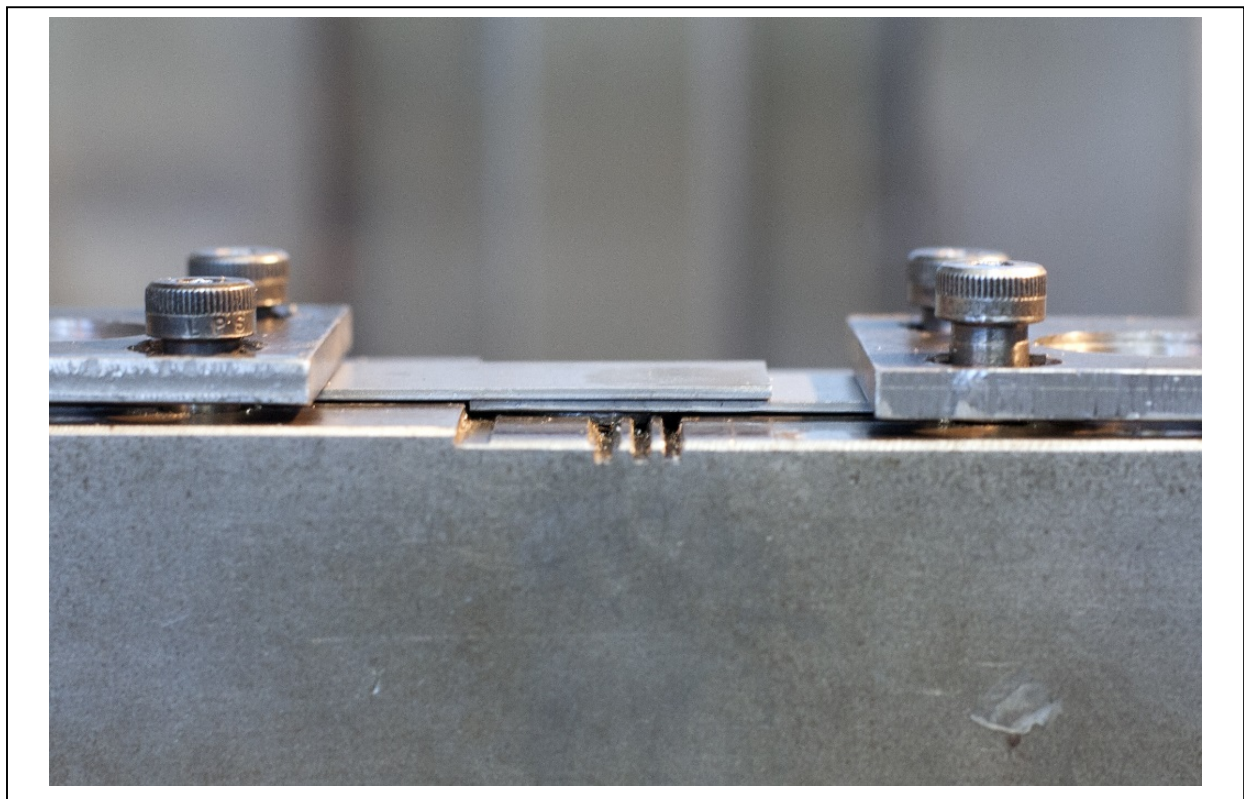
Figure 3-3 Fixture Setup

The DP 980 steel composition in weight percent, were 0.15% C, 1.44% Mn, 0.011% P, 0.007% S, 0.32% Si, and 0.02% Cr, where the balance was Fe. Welds were performed on the Fadal CNC Mill with the different rpms as shown in the Table 3-1. Previously, the thermocouples were placed flat underneath the bottom plate. This resulted in the welding of thermocouples, creating cavity, and disturbing material flow as shown in Figure 3-6.

(a)	(b)	(c)

Figure 3-4 (a) Thermocouple Placement (b) Before Welding (c) After Welding

Figure 3-5 Thermocouple Welded on the Bottom Coupon Because of High Heat
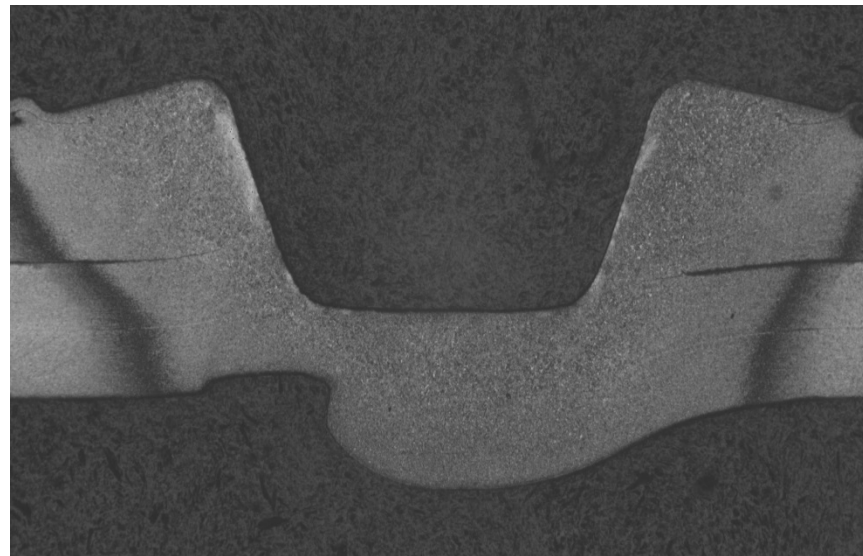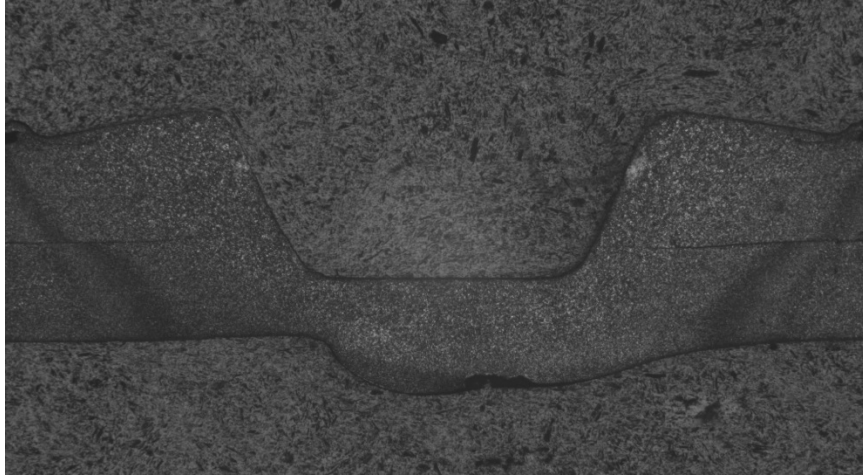
Figure 3-6 Microscopic Images Showing Results of Thermocouple Welding

The anvil was modified to overcome this issue. The modified anvil was divided into three parts for measuring the temperatures at the bottom of the weld. The different parts were:

1. 1.2mm thick plate at the top

2. 1.2mm thick plate with grooves

3. Bottom part

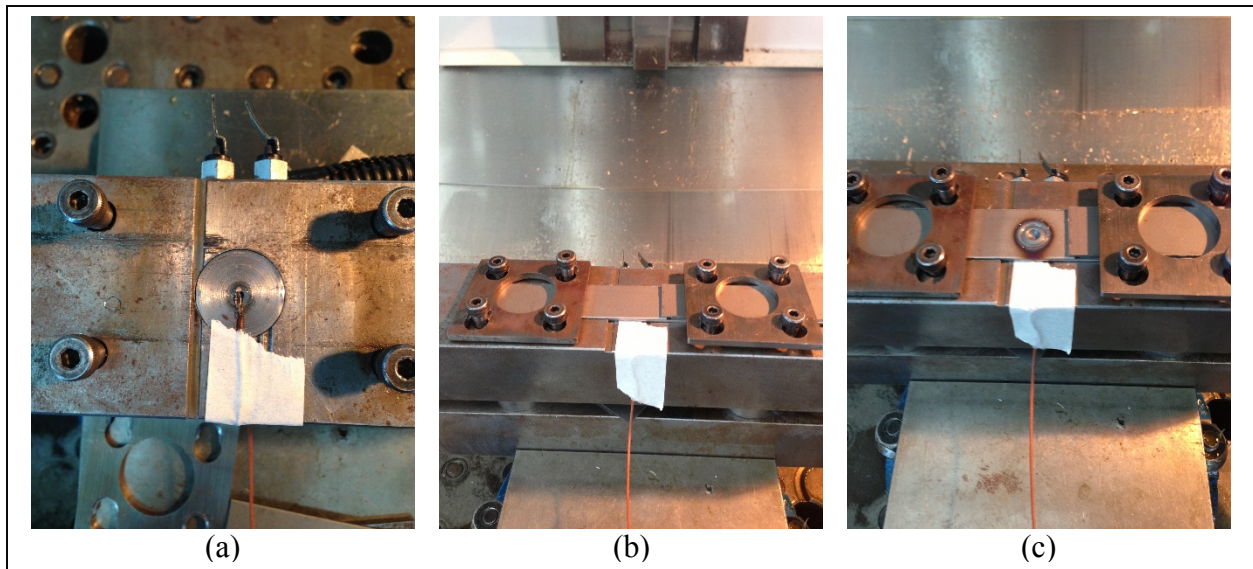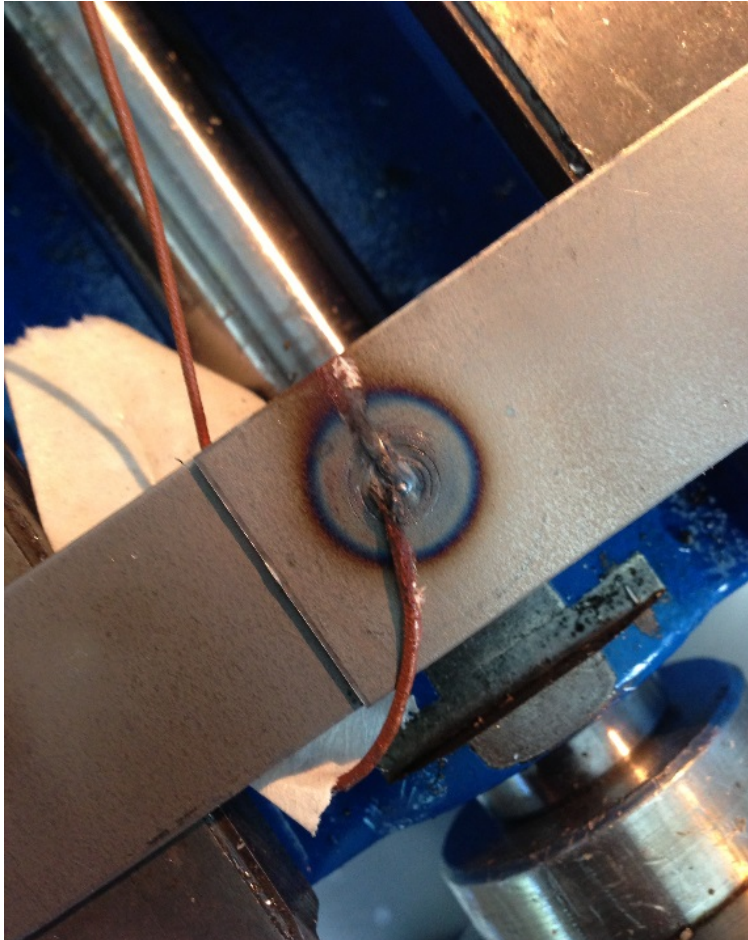To make the welding surface flat, thermocouples were positioned in channels machined on part 2. Three thermocouples were placed at a distance of 3, 4, and 6.5 mm away from the center of the weld along the center axis of the specimen.
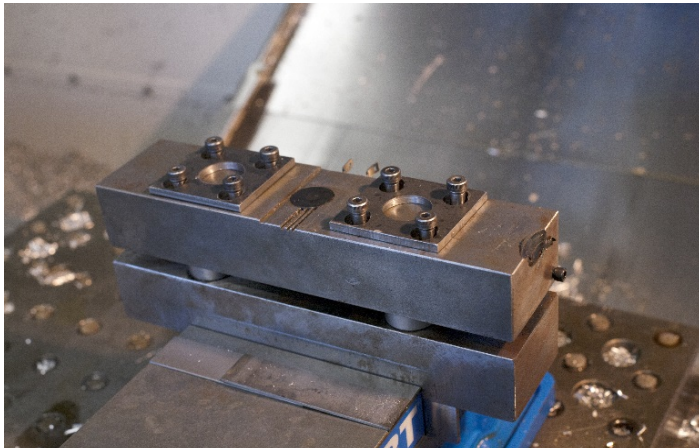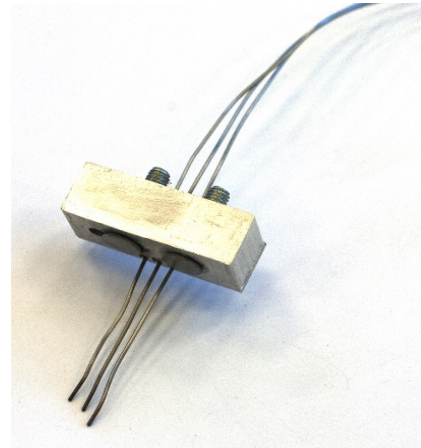
(a)   (b)

Figure 3-7 (a) Fixture with Modified Anvil (b) Thermocouples Locator/Fixture

The Si_3N_4 tool used for the experiment had a concaved shoulder with a 10 mm diameter, and a tapered pin with three small flats at the tip of the pin. It was observed that the flats wore out after a few welds, approximately 5-10 depending mostly on the plunge rate and the rpm. All the experiments were conducted after the flats were worn out, to keep the consistency in the flow

of material. A constant time gap of 5 minutes was kept between the experiments. The experiments were run on Fadal CNC mill.

Figure 3-8 FADAL CNC Mill

The thermocouples were bent and carefully positioned so that they were touching the bottom of the plate 1 constantly. They were checked after three welds to make sure there was no change in their location

The Instron screw-driven frame at a rate of 10 mm/min was used to test the lap shear specimens. Welded samples were sectioned through its center using Sodick Wire Electrical Discharge Machining (EDM).

18
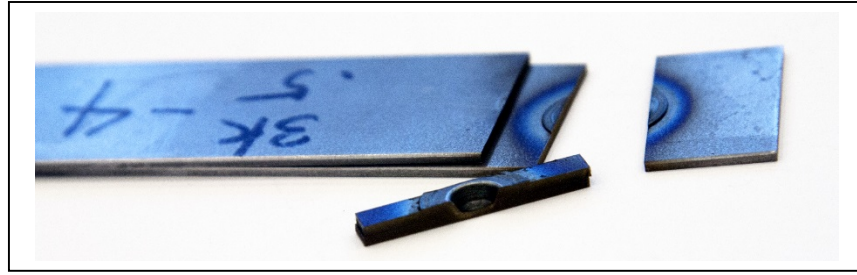
Figure 3-9 Sectioned Welds Using Wire EDM

Metallography samples were mounted in a bakelite material and polished. The polishing process started with 120 grit sand paper, and continued through 240, 400, 600, 800 and 1200 grits. Then it was polished to 6, 3 and 1 micron finish. Etching was performed with 2% Nital solution for 15 seconds, and rinsed in methanol. After the polishing process, images were taken using the optical microscope.

(a)   ....
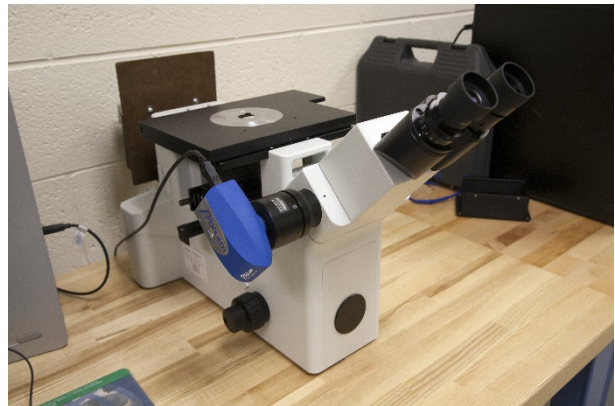
Figure 3-10 (a) Bakelite Samples (b) Optical Microscope

3.4   **Data Collection Methods**

Welding load data was collected using a special fixture with four load cells connected to a data acquisition system with a sampling rate of 100 Hz. The temperature data was collected using a DAQ assistant connected to a program on LabView at 50 Hz. All the data was exported to Microsoft excel and MathWorks MATLAB for data analysis.

(a)   (b)
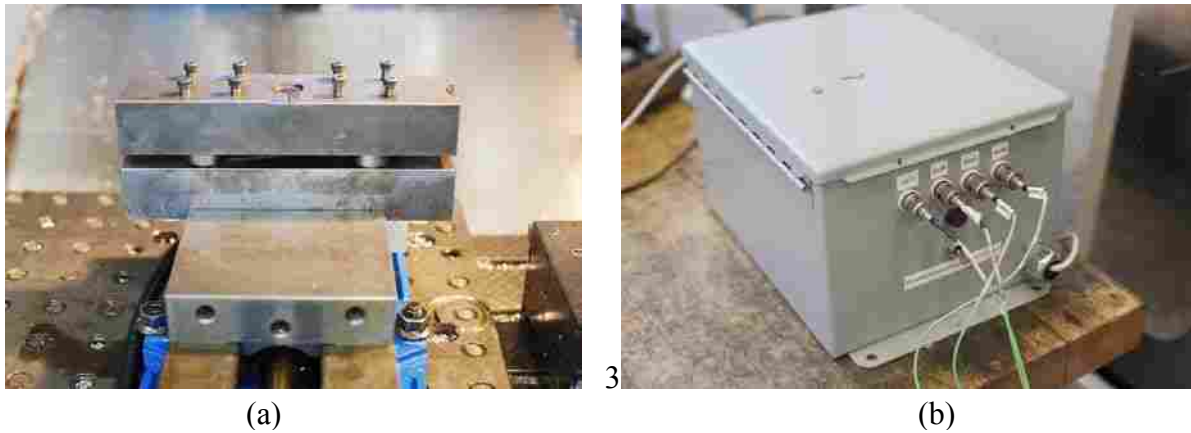
Figure 3-11 (a) Fixture with Load Cells (b) DAQ Assistant for Data Recording

3.5   **FSSW Model**

The 2D axisymmetric FE model of FSSW process was developed using Forge® software. The software was updated with the Lagrangian scheme with explicit time integration, and was used to model the flow of the sheet material as it was subjected to boundary conditions of the rotating tool and the fixed backing plate. The model was done in 2D, but thermo boundary conditions were also modeled which gave an aspect of 3D. Using a 2D velocity field, material flow was calculated. The heat generated by friction was also calculated by using the virtual sliding velocity between the sheet metal and the rotating tool. Using this heat data as boundary

condition allowed for the thermal calculations to be made between the tool and the sheet. The material flow stress as a function of strain, strain rate and temperature was modeled off of the Norton-Hoff law. The expression for the deviatoric stress tensor is shown below:

$$s = 2K\left(\sqrt{3}\,\dot{\bar{\varepsilon}}\right)^{m-1}\dot{\varepsilon} \tag{1}$$

Where $\dot{\varepsilon}$ denotes strain rate tensor, $\dot{\bar{\varepsilon}}$ denotes effective strain rate, K denotes the material consistency, and m denotes the strain rate sensitivity. n is the strain hardening exponent and β is a thermal softening parameter, the material consistency K is a function of temperature T and the equivalent strain $\bar{\varepsilon}$.

$$K = K_0(\varepsilon_0 + \bar{\varepsilon})^n \varepsilon^{\frac{\beta}{T}} \tag{2}$$

While providing the contact stresses with the tool that was used to calculate the friction shear stress, the viscoplastic law was primarily capable of modeling material flow stresses in the region of the weld. The data pertaining to this law was obtained from JmatPro specifically for DP980 steel, for the range of rates and temperature that is encountered during FSSW.

Using a modified Coulomb law, the friction at the sliding interface between the tool and the sheet were modeled. The coulomb friction law modeled shear stress as a function of contact pressure or normal stress. Because this law is often used for room temperature and the standard law does not model the threshold beyond the shear stress saturates at high temperature, a modification is employed as follows:

$$\tau = \mu\sigma_n \text{ while } \tau < \frac{\sigma_0}{\sqrt{3}}, \text{ otherwise } \tau = \frac{\sigma_0}{\sqrt{3}} \tag{3}$$

Where μ denotes the friction coefficient, σ_o denotes the current yield stress of the sheet material, and σ_n denotes the normal stress at the contact surface. By modifying the law, it ensured that the shear stress at the sliding interface would not increase above the yield shear stress of the softer material, which in this case was the sheet.

The flow of material was calculated based on a finite element discretization using an enhanced (P1+/P1) 3-noded triangular element (Forge, 2009). The equilibrium equations were solved at each increment using the Newton-Raphson method. Where the FSSW tool and backing plate were considered rigid, the unilateral contact condition was applied to the sheet surfaces using a nodal penalty formulation. The sheet geometry at each increment of calculation was updated using an explicit time integration scheme.

$$X_{t+\Delta t} = X_t + V_{mesh}\Delta t \tag{4}$$

X denotes the mesh material coordinate, V_{mesh} denotes the component of velocity of the mesh at time t, and Δt denotes the time increment chosen sufficiently small. The evolution of temperature in the tool was modeled in order to provide accurate boundary conditions at the tool/sheet interface. The temperatures in both the FSSW tool and the sheet were calculated at the end of each material flow increment. The calculated velocity field allowed for computing strain rates and stresses in the sheet, which were then used to determine the heat dissipated by friction and plastic deformation. The heat dissipated by plastic deformation (derived from the velocity field) is given by:

$$\dot{q}_v = f\,\bar{\sigma}\,\dot{\bar{\varepsilon}} \qquad (5)$$

Where $\bar{\sigma}$ is equivalent stress. The factor 'f' took into account the fraction of deformation energy converted into heat, taken as 0.9 in this research. For a Norton-Hoff viscoplastic material the heat generation rate from material deformation is computed as follows:

$$\dot{q}_v = f\,K\left(\sqrt{3}\,\dot{\bar{\varepsilon}}\right)^{m+1} \qquad (6)$$

Heat from friction was computed as a function of sliding that occurred along the radial direction of the tool surface, as well as sliding that occurred from rotation, as shown below:

$$\dot{q}_f = \tau \cdot A = \pi r^2 (v_{rad} + v_{rot}) \qquad (7)$$

Where τ is the shear stress calculated from equation 3, v_{rad} is the radial sliding velocity between sheet and tool, calculated from the velocity field in the sheet, and v_{rot} is a virtual rotational sliding velocity between sheet and tool.

The tool, sheet and backing plate were subjected to volume meshing, whereas the tool holder and fixture were surface meshed to reduce the computational time and space requirements. The tool and backing plate had fine mesh; the mesh of the sheet was finer near the contact point with the tool as shown Figure 3-12. Even though the anvil was divided in three parts in the experiment, it was not specified in the model and a single part was used. A total of 4891 elements and 2955 nodes were generated in this model.
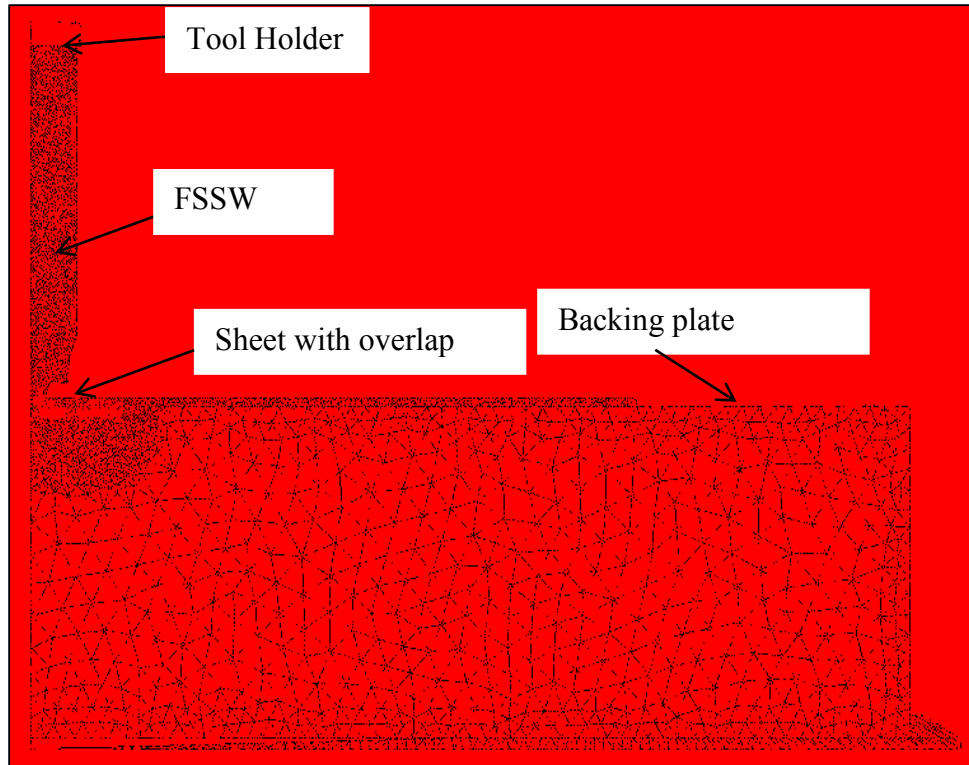
Figure 3-12 2D Model

The model used updated Lagrangian scheme for the sheet material. The remeshing feature provided by Forge® was used to maintain a high quality mesh when the sheet was subjected to severe deformation.

4 RESULTS AND DISCUSSION

4.1 Weld Parameter Development

A simple one-stage plunge with a constant plunge rate was used. Initial tests were run to make sure that the lap shear strength was greater than 5kN. Two plunge rates of 0.106 mm/s and 0.212 mm/s were chosen after the initial tests. Lap shear fracture loads and vertical welding loads as a function of tool rpm and plunge rate are shown in Table 4-1

Table 4-1 Parameter Results

Tool (rpm)	Plunge Rate (mm/s)	Lap Shear Fracture Load (kN)	Vertical Welding Load (kN)
3000	0.106	6.1	7.2
3000	0.212	8.6	3.4
4000	0.106	7.6	5.4
4000	0.212	8.2	4.4
5000	0.106	7.8	5.9
5000	0.212	9.5	5.0
6000	0.106	7.0	5.6
6000	0.212	5.7	4.8

For given plunge rates, 5000 rpm resulted in high lap shear fracture loads for both the plunge rates. Previous experiments with single feed rate resulted in more heat and lower vertical welding loads for higher levels of rpm. The data shown in table above does not correlate to that; it is random, which might have resulted from the randomization of experiments and tool wear.

4.2   Tool Wear

The tool contained three small flats, but these flats tended to wear off depending mostly on the plunge rate they were run on. The randomization of test removed the effect of the flats on the measurements. After few experiments, the flats were completely removed leaving a completely smooth pin. Images of the new and used tool are shown in Figure 4-1.
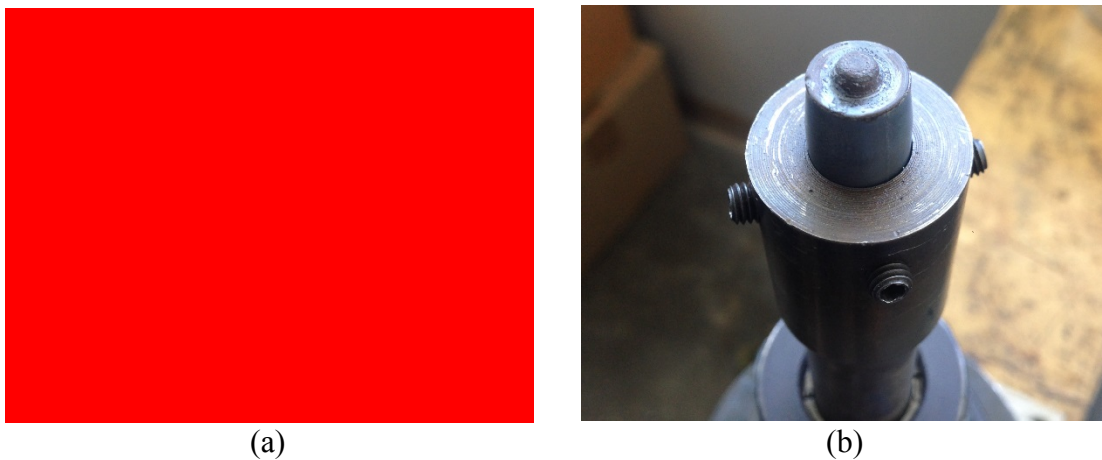

(a)   (b)

Figure 4-1 (a) New Tool (b) Used Tool with Flats Worn Out

4.3 Aesthetic Quality of the Weld

It was found that the welding time had a significant effect on the TMAZ and HAZ of the weld. Longer welding times caused higher heat generation and material stirring, resulting in a larger HAZ zone. Low plunge rate and low RPM resulted in the larger HAZ zone.

4.4 Numerical Model Temperature Predictions

The model employed 4,695 linear triangle elements for the tool and 12,543 linear triangles for the sheet. The sheets were modeled as one single body with a thickness of 2.4 mm at the overlap area and 1.2 mm on the rest in order to simplify the contact problem. Virtual Lagrangian sensors were placed to track the interface between the sheets as a function of deformation. The sheet was set up to automatically remesh when the distortion reached a prescribed level. During the course of simulation, this led to small variations in the number of elements in the sheet mesh. The room temperature was considered to be 25°C. The backing plate was assumed to be rigid, and the mass of the backing plate was relatively large compared to the mass of the sheet. The heat transfer coefficient between the tool and the sheet was 20,000 W/m^2-°C, and the coefficient between the sheet and the backing plate was 2,500 W/m^2-°C.

A magnified image of the model with the position of thermocouples is shown in Figure 4-2. The measurements were compared with the predicted temperatures for the model validation.

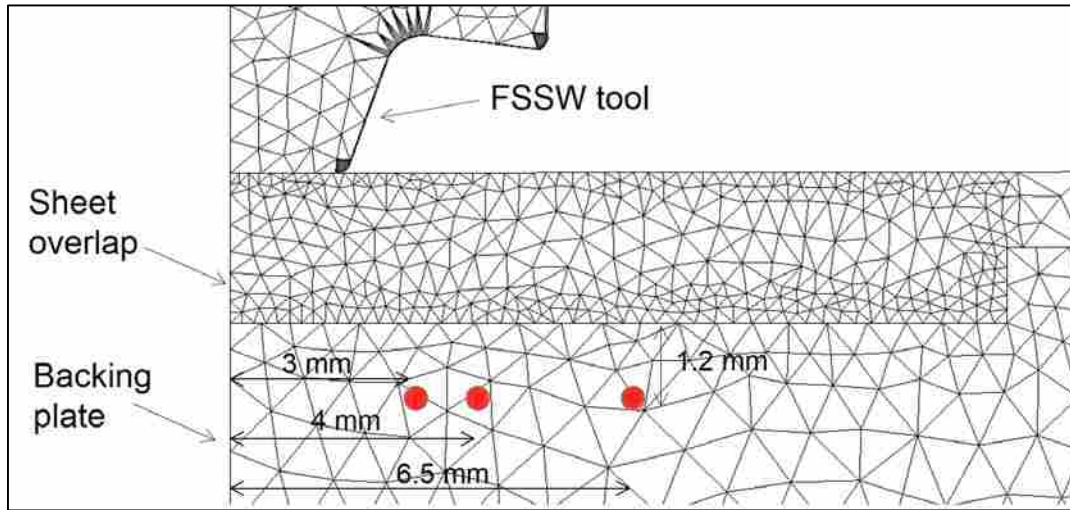**Figure 4-2 Schematic Showing the Locations of Temperature Sensors**

Even though during the experiments the plunge depth was set to 2.4 mm, the average depth was measured to be 1.9 mm. So for the simulation, the depth of 1.9mm was used with a friction coefficient of 0.35. Three temperature measurement replications were performed at a constant tool speed of 5000 rpm and a constant plunge rate of 0.42 mm/s.

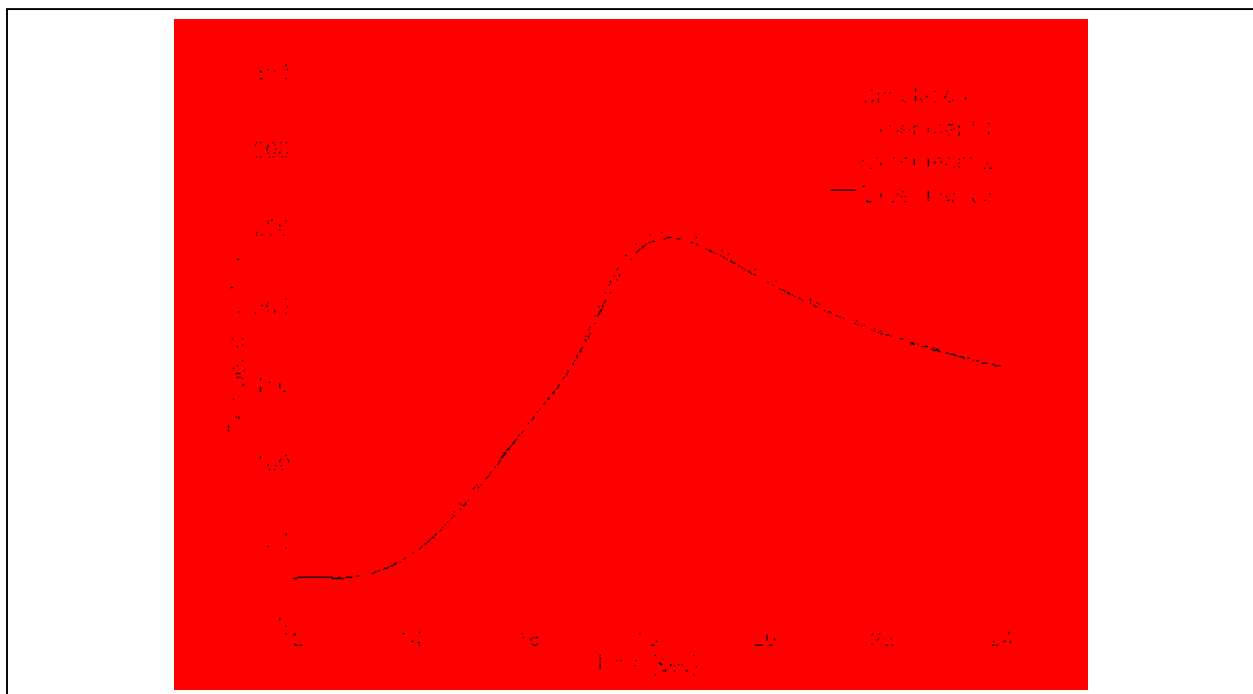**Figure 4-3 Experimental and Predicted Temperatures at 3mm from the Center**

Figure 4-4 Experimental and Predicted Temperatures at 4 mm from the Center

29
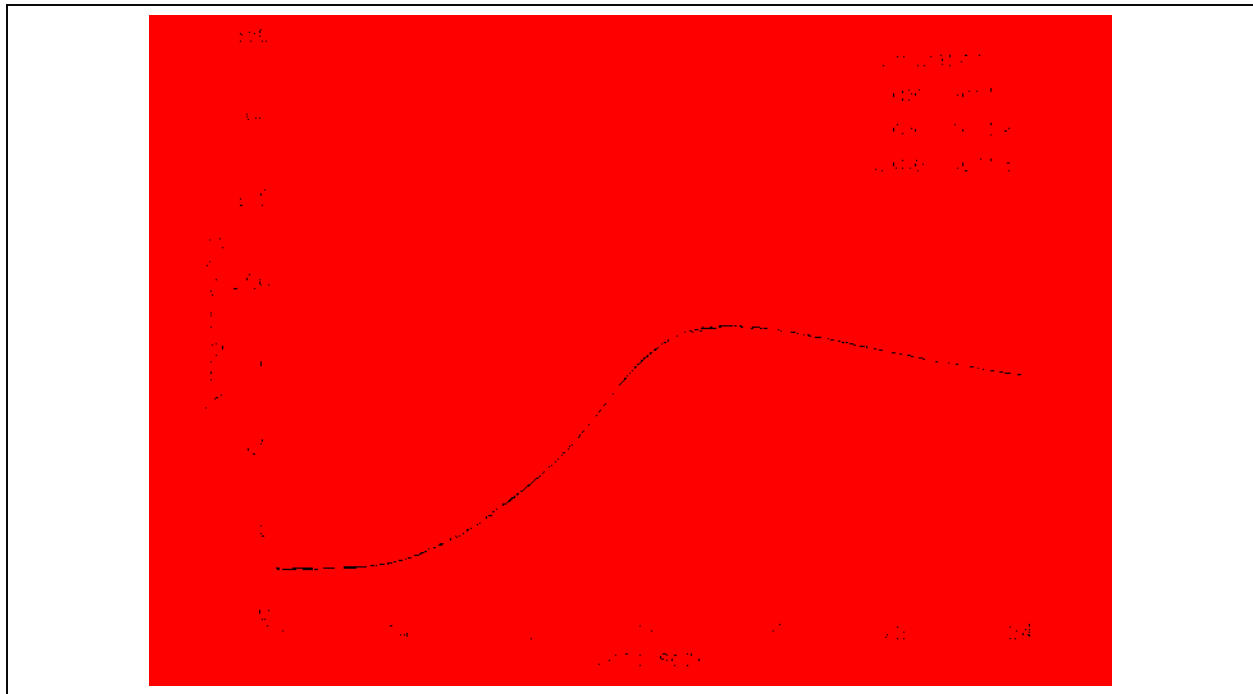
Figure 4-5 Experimental and Predicted Temperatures at 6.5 mm from the Center

The peak temperatures and the temperature-time curves from the experiments were very close to the ones from the simulation as summarized in Table 4-2.

Table 4-2 Comparison of Average Peak Temperature with Predicted Temperature

Distance from the weld center	3mm	4mm	6.5mm
Experiment 1	302.3	253.4	170.2
Experiment 2	294.7	246.6	171.1
Experiment 3	297.4	242.6	171.9
Average	298.1	247.5	171.1
Predicted Temperature	296.0	256.9	167.3
Difference	1%	-4%	2%

Figure 4-6 Temperature Across Different Areas During Simulation

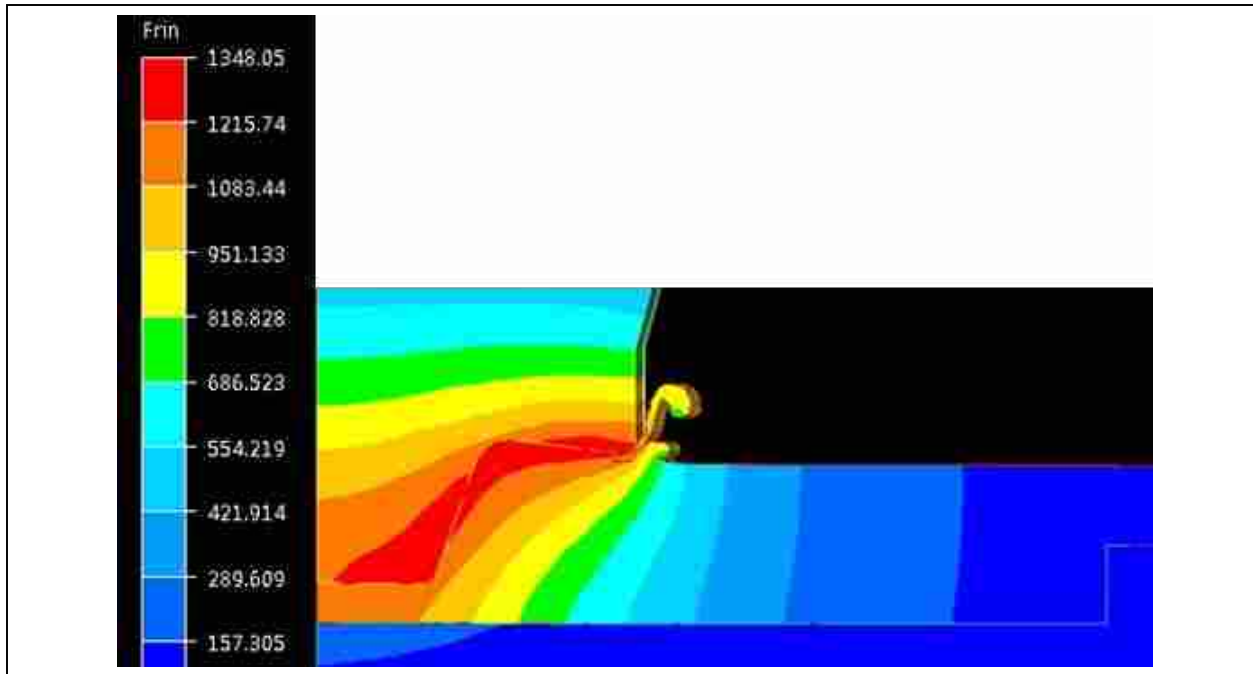## 4.5 3D and 2D Model

Comparison of welding load, friction power along with the effect of plunge rate are covered in this section.

4.5.1 Welding Load Comparison

One of the main issues with the 2D simulation was the overestimation on the welding load prediction compared to the experiments. The welding load was the vertical load required to plunge the tool to a specific depth of penetration. The 3D model was created using the Forge® software and ran for comparison with the 2D model. The primary purpose was to see the differences in the load predictions. It was found that the loads predicted by the 2D were also higher than the ones

predicted by 3D simulation. It took approximately 3 weeks for 3D model to run (using an Intel i7 2820 QM CPU, with 4 cores).

The volume of the sheet was remeshed frequently in order to avoid excessive mesh distortions using a Langrangian framework. The simulation did not run to completion because of the element degeneration and contact difficulties of the flash that formed under the shoulder of the tool. From a practical view point, the implicit solver makes the 3D calculation prohibitive. The partially completed 3D simulation is shown in the Figure 4-7.

Although, the 3D simulation did not run all the way, it helped in partial comparison of the welding load predictions with the 2D model. The comparison of the 3D and 2D welding loads is shown in Figure 4-8.
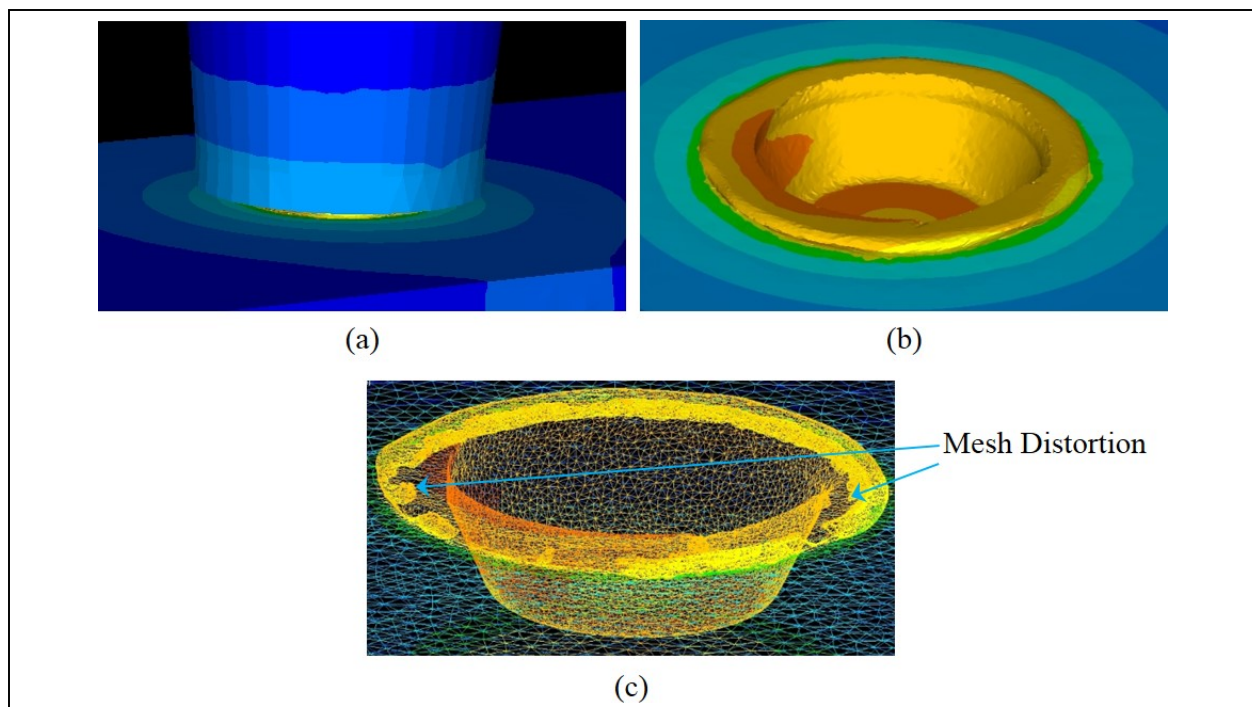

(a)

(b)

Mesh Distortion

(c)

Figure 4-7 Initial Contact (b) Temperature Gradients (c) Mesh Distortion
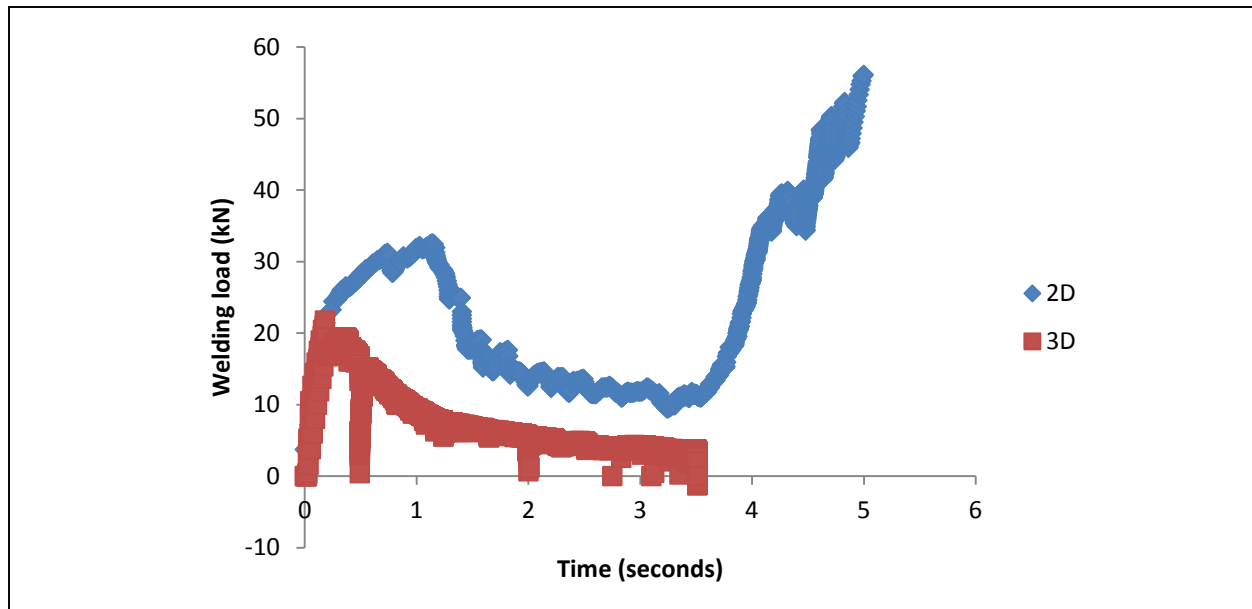
Figure 4-8 Welding Load vs. Time

The peak loads using the tool speed of 5000 rpm, the constant plunge rate of 0.42 mm/s, the plunge depth of 1.9 mm and the friction coefficient of 0.35 were between 9-12 kN. From Figure 4-8, we can see that both models over predicted the loads. But the predictions from 2D are much higher than those from 3D. The difference might have resulted from the lack of component in the velocity field. There is no rotation in the 2D model; it is essentially simulating the plunge of a non-rotating tool that is heating as if it is rotating at 5000 rpm. Whereas in the 3D, the tool is rotating; and therefore it includes the shearing of sheet material close to the tool surface by friction.

4.5.2 Friction Power Comparison

Prior modeling work on the FSSW has shown that there are two sources of heat: friction and plastic deformation. Friction is the primary source that accounts for about 97% of the heat

33

produced during the process. The fact that heat is generated from the rotational sliding of the tool on the sheets was assumed in the 2D model. The surface speed of the tool was used to calculate the heat as shown previously in equation (7), presented again here:

$$\dot{q}_f = \tau \cdot (v_{rad} + v_{rot}) \tag{7}$$

Where τ is the shear stress calculated from equation (3), v_{rad} is the radial sliding velocity between the sheet and the tool, calculated from the velocity field in the sheet, and v_{rot} is a virtual rotational sliding velocity between the sheet and the tool. A comparison between 2D and 3D friction power in shown in the Figure 4-9.
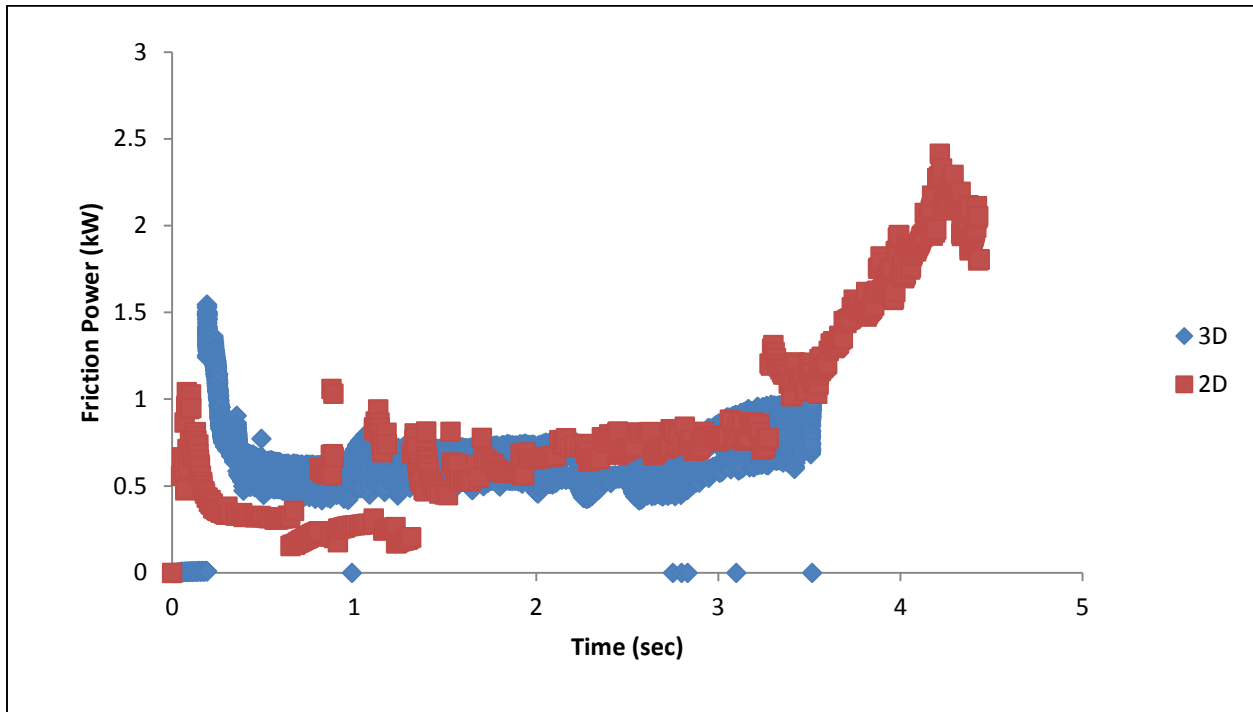

Figure 4-9 Friction Power vs. Time

A very small difference was observed between 2D and 3D results that were run under the same conditions. Contact conditions between the sheet and the tool evolved as the simulation continued, which included slight difference in contact after remeshing. This might be the reason for the scattering of the data. Since, the 3D simulation did not run all the way to the end, a stable time period from 1.5 to 3 seconds was chosen for the comparison. Based on the averages over this time span, the 3D model had 3% less friction power than the 2D model. The 3D model had 96.2% heat generation from friction and 3.8% from the plastic deformation. On the other hand in the 2D model, 97.9% of the heat generation was from friction and the remaining 2.1% came from the plastic deformation.

4.5.3   Effect of Plunge Rate and RPM

The 2D model was used to predict the effect of tool rpm and plunge rate on welding temperatures at the end of the welding cycle. Two different plunge rates: 0.106 mm/s and 0.212 mm/s were used; the tool speeds ranged from 3000- 6000 rpm. The temperatures were taken from the top and bottom surfaces of the sheet. The trend can be seen in Figure 4-10.
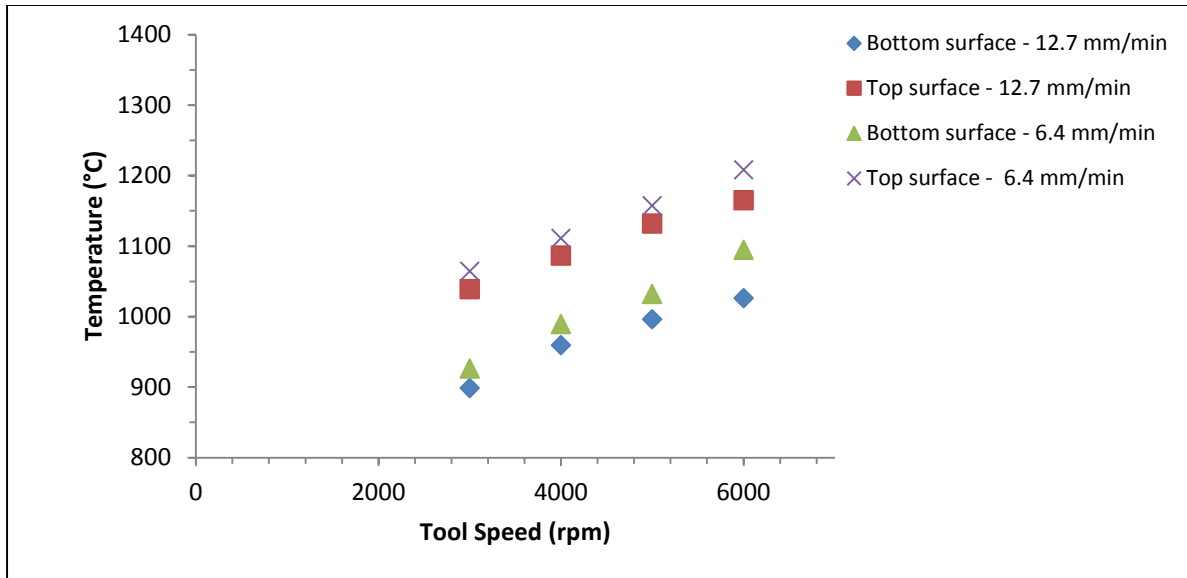
Figure 4-10 Temperature vs. RPM for Two Different Plunge Rates

The temperatures at the end of the welding cycles were directly proportional to the rpm: the higher the rpm, the higher the temperature for a given plunge rate. Also, it was observed that for a given rpm, slower plunge rate resulted in higher temperatures.

4.6   2D Model and Bond Area

In the model a line of Langrangian markers were kept at a distance of 1.2mm from the surface, which is the thickness of the sheet. The markers moved with the flow of material and the movement was tracked throughout the simulation. They were updated at each increment of the simulation. Figure 4-11 shows the movement of the markers from start to the end of the simulation.

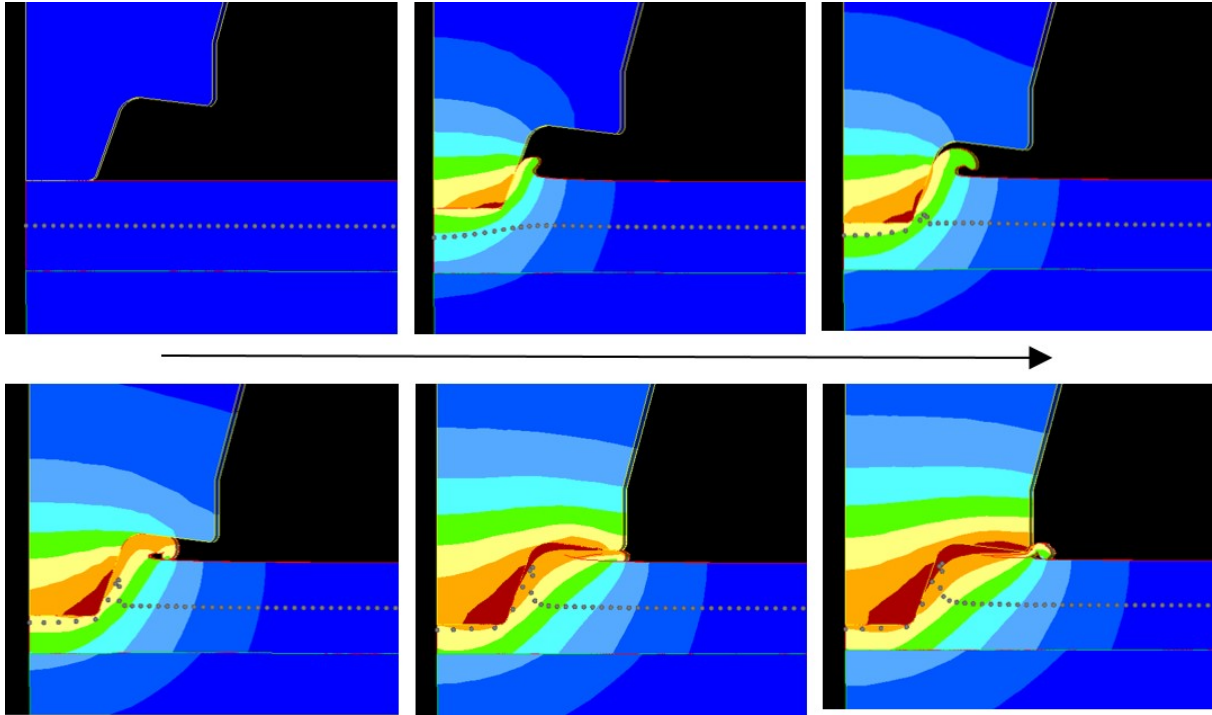**Figure 4-11 Movement of Langrangian Markers During the Welding Process**

From the start to the end of the welding process, the 2D model predicted the joint line movement reasonably. As can be seen in the Figure 4-11, the joint line started curling up as the welding process progressed and formed a hook at the end. A comparison between the shape of the interface from the simulation and the experiment is shown in the Figure 4-12.
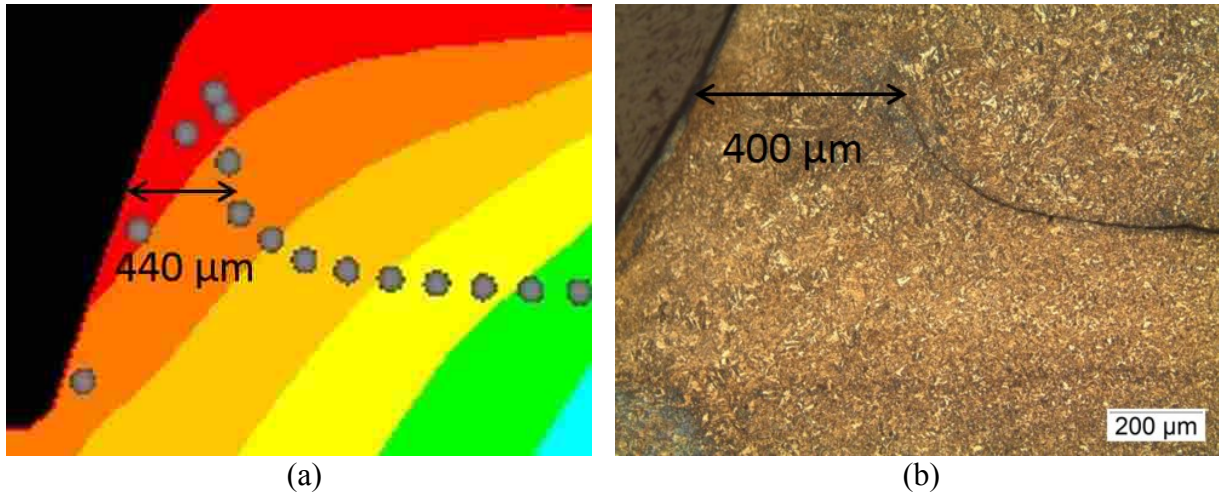
Figure 4-12 Joint Shape Interfaces from Simulation and Experiment

The joint line was present in the model from start to the end of the welding process, but it was not visible in the experiment. The vanishing of the portion of the interface was due the bonding that takes places in weld zone. So, the model did not reflect the bonding that occurs during the welding process. There was a reasonable prediction of the shape and position of the hook. The distance from the edge to the hook computed from the model was measured and found to be within 10% of the experiment.

5 CONCLUSIONS AND RECOMMENDATIONS

5.1 Conclusions

The simplified 2D, axisymmetric finite element approach was able to predict the evolution of the joint interface along with the shape and position, with a reasonable level of accuracy. The model was used to predict the peak temperatures at three different positions from the center of the weld. The amount of heat generated on both the 2D and 3D models differed by a few percentage points. The values were close to the heat generation of 97% from friction that was observed on the FSSW of aluminum (Awang, 2010).

The experimental and the 2D modeling work done for this thesis has provided support for the hypothesis that the joint interface along with the peak temperatures can be predicted by the 2D model within 5-10% difference. The model can be an effective tool in understanding the behavior of other materials apart from DP 980 steel during the FSSW process. Various parameters can be changed to different settings in order to find out their impact on the results.

5.1.1 Temperature Predictions

The peak temperatures were predicted within 5% range when compared to the experimental data. The greatest difference was 4% between the model prediction and the experiment. Also, the slope of predicted the time- temperature curves were reasonably close to the experiment.

5.1.2 Joint Interface Prediction

When compared to the experiment, the evolution of the interface between the sheets was predicted to within 10% by the 2D model. The model helped to visualize the movement of the joint line and the formation of the hook over the course of tool plunge. The flashes seen at the end of the simulation looked very similar to the one from the experiment. This increased the validity of the model.

5.2 Recommendations

Recommendations for further research include further 2D and 3D model development, tool design, and tool material development in order to reduce the tool wear. Also, parameter optimization can be a good area to be considered. In this research, only lap shear testing was conducted to measure the strength of the joint. In the future, it is recommended that cross tension testing, fatigue testing, and other feasible testing methods should be used to gather information on the strength of the joint.

5.2.1 2D and 3D Model Further Development

The prediction of welding loads was significantly higher by the 2D as well as the 3D model. The 2D model was unable to simulate the shear force caused by the rotating tool. Close comparison between loads measured during the experiment and the models (2D and 3D) is required in order to predict the welded bond area. Better understanding of the relationship between time, temperature, and pressure will allow for the close prediction of the bond area and corresponding strength of the joint.

5.2.2   Tool Design and Tool Material Development

A concave shoulder tool with flats on the pin was the only tool used in this study. Flats wore out very quickly and it was noticed that there was a gradual decrease in the strength of the joint when the experiments were run under constant parameters. Si_3N_4 tools tend to wear out quickly, especially when run at a slow plunge rate. New tool designs and new materials should be investigated, which can improve the tool life and make the FSSW process more feasible for industrial applications.

5.2.3   Parameter Optimization

The relationship between rpm, plunge rate, and plunge depth on the life of the tool and strength of the joint is unknown at this time. New parameter sets should be tested to find out if they have an influence on the life expectancy of the tool. The development of better parameter sets along with the tool design and tool material for the greatest strength of the joint can take FSSW of AHSS to the next level.

REFERENCES

Al-Shahrani, A and B.P. Wynne. "Effect of Dwell Time on Friction Stir Spot Welded Dual Phase Steel." *Advanced Materials Research* 83, (2010): 1143-1150.

Awang, M. and V.H. Mucino. "Energy Generation During Friction Stir Spot Welding (Fssw) of Al 6061-T6 Plates." *Materials and Manufacturing Processes* 25, No. 1-3 (2010): 167-174.

Fanelli, P., F. Vivio and V. Vullo. "Experimental and Numerical Characterization of Friction Stir Spot Welded Joints." *Engineering Fracture Mechanics* 81, (2012): 17-25.

Feng, Z., M.L. Santella, S.A. David, R.J. Steel, S.M. Packer, T. Pan, M. Kuo and R.S. Bhatnagar. *Friction Stir Spot Welding of Advanced High-Strength Steels-a Feasibility Study*. SAE Technical Paper, 2005.

Hirasawa, S., H. Badarinarayan, K. Okamoto, T. Tomimura and T. Kawanami. "Analysis of Effect of Tool Geometry on Plastic Flow During Friction Stir Spot Welding Using Particle Method." *Journal of Materials Processing Technology* 210, No. 11 (2010): 1455-1463.

Miles, M, U Karki and Y Hovanski. "Temperature and Material Flow Prediction in Friction-Stir Spot Welding of Advanced High-Strength Steel." *JOM*, (2014): 1-7.

Muci-Küchler, K.H., S.S.T. Kakarla, W.J. Arbegast and C.D. Allen. *Numerical Simulation of the Friction Stir Spot Welding Process*. SAE Technical Paper, 2005.

Oikawa, H., G. Murayama, T. Sakiyama, Y. Takahashi and T. Ishikawa. "Resistance Spot Weldability of High Strength Steel (Hss) Sheets for Automobile." *Shinnittetsu Giho* 385, (2006): 36.

Ridges, C.S. "Tool Life of Various Tool Materials When Friction Spot Welding DP980 Steel." (2011).

Santella, M., Y. Hovanski, A. Frederick, G. Grant and M. Dahl. "Friction Stir Spot Welding of DP780 Carbon Steel." *Science and Technology of Welding and Joining* 15, No. 4 (2010): 271-278.

Forge 2009, Transvalor Inc. (2009).